GLIA 58:29–42 (2010)

# Axonal Plasticity Elicits Long-Term Changes in Oligodendroglia and Myelinated Fibers

**NINA DRØJDAHL,[1] HELLE HVILSTED NIELSEN,[1] JONATHAN E. GARDI,[2] ANDREAS WREE,[3] ALAN C. PETERSON,[4] JENS RANDEL NYENGAARD,[2] JOËL EYER,[5] AND BENTE FINSEN[1]***

[1]*Medical Biotechnology Center, University of Southern Denmark-Odense, Odense C, Denmark*
[2]*Stereology and Electron Microscopy Research Laboratory and MIND Center, Århus University, Århus, Denmark*
[3]*Institute of Anatomy, Rostock University, Rostock, Germany*
[4]*Laboratory of Developmental Biology, Royal Victoria Hospital, McGill University, Montreal, Quebec, Canada*
[5]*Laboratoire de Neurobiologie et Transgenese, UPRES-EA3143, INSERM Centre Hospitalier Universitaire, Angers, France*

*KEY WORDS*
myelination; sprouting; entorhinal cortex lesion; LacZ transgenic mice; stereology

*ABSTRACT*
Axons are linked to induction of myelination during development and to the maintenance of myelin and myelinated tracts in the adult CNS. Currently, it is unknown whether and how axonal plasticity in adult CNS impacts the myelinating cells and their precursors. In this article, we report that newly formed axonal sprouts are able to induce a protracted myelination response in adult CNS. We show that newly formed axonal sprouts, induced by lesion of the entorhino–hippocampal perforant pathway, have the ability to induce a myelination response in stratum radiatum and lucidum CA3. The lesion resulted in significant recruitment of newly formed myelinating cells, documented by incorporation of the proliferation marker bromodeoxyuridine into chondroitin sulphate NG2 expressing cells in stratum radiatum and lucidum CA3 early after lesion, and the occurrence of a 28% increase in the number of oligodendrocytes, of which some had incorporated bromodeoxyuridine, 9 weeks post-lesion. Additionally, a marked increase (41%) in myelinated fibres was detected in silver stained sections. Interestingly, these apparently new fibres achieved the same axon diameter as unlesioned mice but myelin thickness remained thinner than normal, suggesting that the sprouting axons in stratum radiatum and lucidum CA3 were not fully myelinated 9 weeks after lesion. Our combined results show that sprouting axons provide a strong stimulus to oligodendrocyte lineage cells to engage actively in the myelination processes in the adult CNS. 

## INTRODUCTION

Due to a relatively poor regenerative capacity of injured CNS axons, most studies of neuronal regeneration have up till now focused on the inhibitory effect of myelin proteins on axonal growth (Kapfhammer, 1997; Koprivica et al., 2005; Lee et al., 2007; Schwab, 2004). Less attention has been given to the ability of the regenerating axons to induce a myelination response (Butt and Berry, 2000), that will endow fibres with the capacity for saltatory impulse conduction. While neuronal regeneration refers to the reestablishment of formerly injured neuronal connections, neuronal plasticity also comprises the structural reorganization that leads to formation of new connections formed by axonal sprouts (Will et al., 1985). Although, predominant during development, axonal sprouting and elongation also occurs in response to axonal loss in adult CNS (Carmichael et al., 2001; Deller and Frotscher, 1997; Noppeney et al., 2005; Steward and Vinsant, 1983), when an injured axon may sprout and regenerate, or neighboring intact axons may sprout and elongate to innervate the deafferented target neurons (Seil, 1989).

Axons regulate myelination in the developing CNS (Barres and Raff, 1993; Burne et al., 1996; Kim et al., 2003; Trapp et al., 1997), and maintenance of myelin in the adult CNS (Polito and Reynolds, 2005). Axonal impulse conduction is linked to induction of myelination (Demerens et al., 1996), and axon caliber and growth factors play a major role for the final thickness of the myelin sheath (Cellerino et al., 1997; Fanarraga et al., 1998; Mihailov et al., 2004; Smith et al., 1982). Whereas, proliferation of oligodendrocyte progenitors and their differentation into premyelinating oligodendrocytes takes place in vitro in the absence of axons (Bansal and Pfeiffer, 1985; Knapp et al., 1987; Szuchet et al., 1986), axons are required for formation of myelin sheaths (Demerens et al., 1996; Lubetzki et al., 1993; Noppeney et al., 2005; Wang et al., 2007). Similar mechanisms may also be responsible for the continued myelination of some neocortical regions in adolescents and adults (Baumann and Pham-Dinh, 2001; Benes et al., 1994; Yakovlev and Lecours, 1966), and for the myelination response, that is assumed to take place in brain regions with injury-induced axonal sprouts.

The hippocampus is unique from a plasticity point of view. The hippocampal dentate gyrus shows life-long

Nina Drøjdahl and Helle Hvilsted Nielsen contributed equally to this work.

Grant sponsors: The Foundation of 17.12.1981; The Faculty of Health Science-University of Southern Denmark; The Family Hede Nielsen's Foundation; Retired President Leo Nielsen and Wife Karen Margrethe Nielsen's Foundation for Basic Health Science; The Danish Multiple Sclerosis Society; Warwara Larsens Foundation; Lily Benthine Lunds Foundation; Director Ejnar Jonassons Foundation; A. J. Andersen Foundation; The Novo Nordic Foundation; The Lundbeck Foundation; The Danish MRC.

*Correspondence to: Bente Finsen, Medical Biotechnology Center, University of Southern Denmark-Odense, Winsloewparken 25, 2 Floor, DK-5000 Odense C, Denmark. E-mail: bfinsen@health.sdu.dk

Received 9 July 2007; Accepted 29 April 2009

DOI 10.1002/glia.20897

Published online 19 May 2009 in Wiley InterScience (www.interscience.wiley.com).

neurogenesis (Lledo et al., 2006) and evidence of sprouting of several intrinsic and extrinsic afferent fibre systems following injury (Deller and Frotscher, 1997; Steward and Vinsant, 1983). This plasticity also extends to the CA3 pyramidal cells, that give rise to the highly collaterized CA3-associated fibre system. Notably, these axons sprout after Schafferotomy or kainic acid induced chronic epilepsi (Dinocourt et al., 2006; Siddiqui and Joseph, 2005). In addition, although not directly affected by transection of the entorhino–hippocampal perforant pathway (PP), PP deafferentation leads to sprouting of CA3-associated Timm-stained, zink-containing nerve fibers within the CA3 (Drøjdahl et al., 2002; Zimmer et al., 1974). Observations of transiently increased myelin basic protein (MBP) mRNA levels in oligodendrocytes in stratum radiatum and stratum lucidum CA3 (srl-CA3) in PP deafferented hippocampus indicate that sprouting of the CA3-associated fibres might induce a myelination response (Drøjdahl et al., 2004; Jensen et al., 2000b).

In this study, we investigated the capacity of the oligodendrocyte lineage to myelinate newly formed, axonal sprouts in the adult CNS. For this we combined the use of a transgenic oligodendroglial marker, silver-staining of myelinated axons and design-based stereological methods to estimate changes and in the length of myelinated fibres (Larsen et al., 1998) and in oligodendrocyte numbers (Dorph-Petersen et al., 2001; Gundersen, 1986; West et al., 1991;) in the srl-CA3 of the adult mouse following PP transection. Furthermore, myelin sheath properties were evaluated by electron microscopy and oligodendrocyte formation by incorporation of the thymidine-analogue, bromodeoxyuridine into their DNA during mitosis. The results of the study show that axonal lesion-induced sprouting of CA3-associated fibres is accompanied by a significant increase in the total length of myelinated axons, with reduced myelin thickness, and in increased total numbers of oligodendrocytes 9 weeks after lesion.

## MATERIALS AND METHODS

### Mice

MBP-LacZ transgenic (tg) mice expressing *E. coli* LacZ under the control of a 9.6 kb MBP promoter leading to production of β-galactosidase (β-gal) in oligodendrocytes were used (Foran and Peterson, 1992). The mice were on a mixed genetic background (C57BL/6 × C3H) (Foran and Peterson, 1992), but similar to C57BL/6 mice in terms of pattern of myelination and response of $NG2^+$ cells to PP lesion (Drøjdahl et al., 2004; Nielsen et al., 2006). For the quantitative analysis young adult male tg mice were used. In addition, young adult tg mice of mixed sexes, and young adult male C57BL/6 mice obtained from Bomholtgaard A/S, Denmark, were used for studies of the NG2 cell response and cell proliferation or electron microscopy. Mice were housed under a 12 h light-dark diurnal cycle with food and water ad libitum and handled in accordance with the guidelines of The National Danish Animal Care Committee.

### Surgery and Bromodeoxyuridine Injection

Axonal sprouting in the srl-CA3 of the right hippocampus was induced by transection of the entorhino–hippocampal PP-projection (see Fig. 1) (Drøjdahl et al., 2002; Zimmer et al., 1974), performed as previously described (Drøjdahl et al., 2004). Mice used for studying cellular proliferation following PP transection were divided into three groups. One group of mice, used for determination of the optimal interval for injection of 5-bromo-2′-deoxyuridine (BrdU) received i.p. injections of BrdU (Sigma, Denmark) in an isotonic saline solution (50 mg BrdU/kg) with 8 h intervals starting 48 h prior to sacrifice which took place either at 2, 3, 5, 7, and 10 days after surgery (3–4 mice in each group). The other two groups of mice, that were used for quantitation of BrdU-incorporating cells, received i.p. injections with BrdU with 8 h intervals starting from 24 to 72 h, or 48 to 72 h after lesion and were allowed to survive for 7 days, or for 3 days or 9 weeks ($n$ = 7–8 in each group) after PP transection, respectively. Additional animals were operated and allowed to survive 9 weeks along with their unoperated controls ($n$ = 2–3 in each group) before their brains were processed for electron microscopy. Sham operated mice were sutured after touching of the dura with the wire knife.

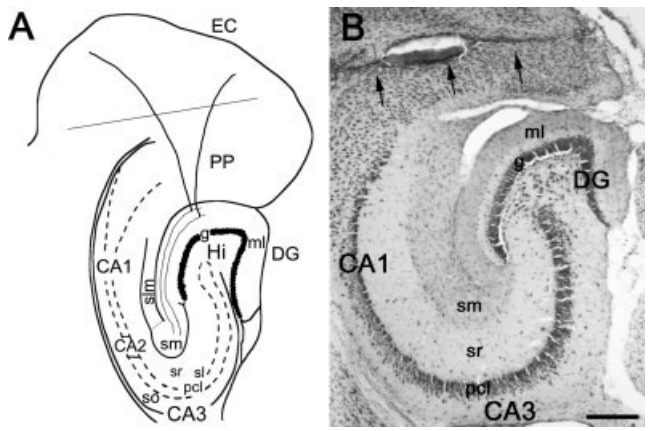


Fig. 1. The hippocampal formation. (**A**) Schematic drawing. The PP projection originates in the entorhinal cortex (EC) and terminates in the molecular layer of the DG and stratum moleculare of the CA3. The line indicates the PP transection site. (**B**) Toluidine blue staining 5 days after PP lesion, showing the location of the wire-knife cut in the EC (arrows). In contrast to the apparently unaffected stratum radiatum (sr) and stratum lucidum (sl) of CA3 (srl-CA3), there is an increased cellularity in the deafferented termination fields; the outer 2/3 of the molecular layer of the DG and the stratum moleculare of the CA3. The increased cellularity in stratum lacunosum-moleculare of the CA1 is caused by the simultaneous transection of the tempero-ammonic tract. Modified from Amaral and Witter (1995). CA1, CA3, regio superior and inferior hippocampus, respectively; DG, dentate gyrus; EC, entorhinal cortex; g, granule cell layer; Hi, hilus; ml, molecular layer; pcl, pyramidal cell layer; PP, perforant pathway projection; sl, stratum lucidum; slm, stratum lacunosum-moleculare; sm, stratum moleculare; so, stratum oriens; sr, stratum radiatum. Scale bar: 100 μm.

## Light microscopy

### Tissue preparation

Mice were deeply anaesthesized with pentobarbital and perfused through the heart with 5 mL phosphate buffer (PB) (0.03 M $KH_2PO_4$, 0.12 M $Na_2HPO_4$, pH 7.4), followed by 20 mL 4% paraformaldehyde (PFA) in 0.15 M PB. Brains were post-fixed 1 1/2 h in 4% PFA, immersed in 20% sucrose in 0.15 M SB at 4°C o.n., and frozen in $CO_2$ snow. Frozen fixed brains were cut horizontally in a cryostat in 8 series of 30 μm (for stereological quantification) or 16 μm (for conventional cell quantification) thick sections. The brains obtained from the BrdU-injected mice with 9 weeks survival were cut into 6 series of 50 μm sections on a Leica VT1000S vibratome (Nussloch, Germany), as described in Wirenfeldt et al., 2003.

### Toludine blue staining

For selection of mice with successful PP-lesions and guidance during delineation of the srl-CA3 sections parallel to those used for quantification were stained with toluidine blue using routine protocols.

### Myelin silver staining

The myelin silver staining resulted in a black staining of myelinated fibres, and was performed as previously described (Drøjdahl et al., 2002).

### β-Galactosidase histochemistry

Sections were dried at RT and immersed in a freshly made solution of substrate. This solution contained 6.67 mg X-gal (5-bromo-4-chloro-3-indolyl-β-D-galactopyranoside) (B4252, Sigma, Denmark) that was dissolved in 1 mL dimethylformamide and added to a mixture of 3.1 mM potassium hexacyanoferrat (II) trihydrat, 3.7 mM potassium hexacyanoferrat (III), and 0.1 M PB with 0.2 mM $MgCl_2$ (Drøjdahl et al., 2004). Sections were developed at 37°C until oligodendrocytes had attained a clear blue color (2 h optimized for counting). Sections were subsequently rinsed in 0.1 M PB for 3 × 5 min, fixed in 4% PFA in 0.1 M PB for 4 h, rinsed 10 min in 0.1 M PB and 2 × 5 min in distilled water, and cover-slipped in Aquatex™ (Merck, Denmark). For more intense staining sections for illustration were incubated with a higher concentration of X-gal (20 mg/mL dimethylformamide).

### Immunohistochemistry

*CD11b/Mac-1.* To validate the PP lesion, sections were stained for CD11b visualizing microglia/macrophages using a rat anti-mouse-CD11b antibody (MCA 711, Serotec, Norway) diluted 1:600, followed by biotinylated goat anti-rat-Ig antibody (RPN 1005, Amersham, Denmark) diluted 1:200 and horseradish peroxidase conjugated streptavidin for enzymatic DAB development according to Drøjdahl et al. (2004).

*NG2.* NG2-expressing cells were visualized using the CD11b/DAB procedure but using a polyclonat rabbit anti-rat-NG2 antibody (AB5320, Chemicon Int.) (diluted 1:500) followed by biotinylated goat anti-rabbit-IgG antibody diluted 1:200 (RPN 480, Amersham, Denmark).

*Oligodendrocytes and myelin.* Mouse anti-rat-Rip antibody (Developmental Studies Hybridoma Bank, University of Iowa) recognizes 2′,3′-cyclic nucleotide 3′-phosphodiesterase in oligodendrocytes and myelin in rats and mice (Friedman et al., 1989; Wanatabe et al., 2006). A biotinylated antibody was kindly donated by Trevor Owens, McGill University. Staining was performed using the DAB procedure described by Drøjdahl et al. (2004) (dilution Rip antibody 1:50).

*Myelin basic protein.* The polyclonal rabbit anti-human-MBP antibody visualizes oligodendrocytes and in particular myelin (A0623, Dako A/S, DK). Primary antibody was applied in a 1:1,000 dilution. Secondary alkaline phosphatase (AP)-conjugated goat anti-rabbit-IgG antibody (A3812, Sigma, Denmark) was applied in a 1:100 solution, followed by rinsing, adjustment of pH to 9.5 in a Tris-HCl buffer and incubation in AP developer (Jensen et al., 1999).

*Controls.* Antibody specificity was verified using an inert isotype control antibody (rat IgG2b, IG-851125, Nordic Biosite AB, Sweden) or serum (rabbit serum, O902 Dako, Denmark) in the same concentration as the primary antibody, or by omission of the primary antibody from the incubations.

### Double-stainings

*BrdU/NG2.* To detect proliferating $NG2^+$ cells, sections from mice injected with BrdU were first stained for NG2 (see above). Sections were thereafter rinsed in 2× SSC (300 mM NaCl, 30 mM sodium citrate, pH 8.0) for 2 × 15 min at RT, incubated in a 49% solution of formamide in 2× SSC for 2 h at 60°C, rinsed in 2× SSC for 2 × 5 min at 60°C, and then incubated in 2 N HCl in 0.05 M TBS for 30 min at 37°C. Sections were then rinsed and incubated with monoclonal rat-anti-BrdU antibody (AB6326, Abcam Ltd., Great Britain) diluted 1:100, which was detected using biotinylated goat-anti-rat-Ig antibody (RPN 1005, Amersham, Denmark) diluted 1:200, and AP conjugated streptavidin (P0396, Dako A/S, Denmark) and incubated in an AP-developer.

*BrdU/β-gal.* To detect proliferating $\beta\text{-gal}^+$ cells, sections from mice injected with BrdU were stained for β-gal (10 mg X-gal/mL dimethylformamide) followed by staining for BrdU as described above but leaving out the step of inactivation of endogenous peroxidases.

*β-gal/NG2 or β-gal/Rip.* Sections were stained for NG2 or Rip with the CD11b/DAB procedure. After rinsing in TBS, the sections were stained for β-gal (10 mg X-gal/ml dimethylformamide) as described above. Control stainings were performed as outlined for individual immunohistochemical stainings.

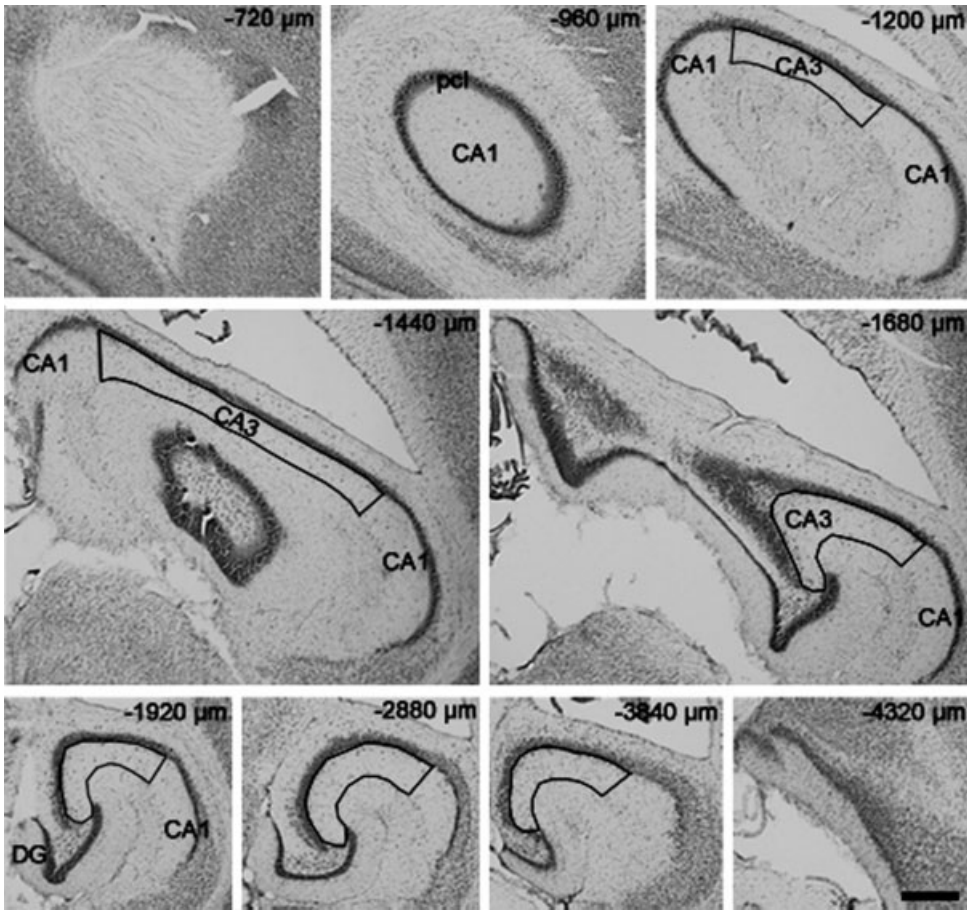


Fig. 2. Low power micrographs of toluidine blue stained sections sampled for stereological sampling within the stratum radiatum and lucidum CA3 (srl-CA3). The framed area shows the srl-CA3 at different dorso-ventral levels of the hippocampus in 30 µm thick horisontal sections from an unlesioned MBP-LacZ-tg mouse. The numbers in upper right corner indicate the dorso-ventral level of the top of the sections relative to the surface of the brain. The sections selected for the illustration were adjacent to the silver and X-gal stained sections used for the stereological quantification of fibre length and oligodendrocyte numbers. CA1, regio superior hippocampus; CA3, regio inferior hippocampus; DG, dentate gyrus. Scale bar: 250 µm.

## Electron Microscopy

For electron microscopy animals were perfused with 5 ml PB followed by 20 mL of chilled 2.5% glutaraldehyde (AppliChem GmbH, Germany) in 0,5% PFA, pH 7.4. Brains were postfixed over night and cut into 50-µm-thick sections on a Leica VT1000S vibratome. Next, tissue blocks containing the right hippocampal formation were generated from mice with complete PP lesions ($n$ = 3), based on evaluation of adjacent Flouro-Jade stained sections (Dissing-Olesen et al., 2007), and from age-matched unlesioned mice ($n$ = 2). The hippocampal tissue blocks were embedded in hydrophilic resin Lowicryl K4M (Electron Microscopy Sciences, Fort Washington, PA). Semi- and ultra-thin sections representing the mid-temporal level of the hippocampus shown in Fig. 1B, were obtained by using a Leica EM FC6 cryo-ultramicrotome. The 1-µm-thick semithin sections were stained with methylene blue-azur II and digitalized and the borders of the srl-CA3 were marked on digitalized images to guide the sampling of the ultrathin sections for electron microscopy. The ultrathin (75 nm) sections were collected on copper grids, counterstained with 5% uranyl acetate and lead citrate, and photographed using a JEOL 100× (Peabody, MA, USA) JEM 2010 electron microscope operated at 80 kV.

## Morphometrical Analysis

### Stereological number, length, and volume estimation

*Sampling*. With the use of an Olympus BH-2 microscope and a digital camera (Color View II), images were projected on a monitor where the PC based Computer Assisted Stereological Toolbox (CAST) Grid software system version 2.3.1.5. (Olympus/Visiopharm, Denmark, modified for global spatial sampling by J. Gardi) was used for sampling. The srl-CA3 was delineated on the screen at the magnification of a 10× objective and counting performed at a 100× oil immersion lens. In the dorsal hippocampus, especially, delineation of the srl-CA3 in the silver and β-gal stained sections was facili-

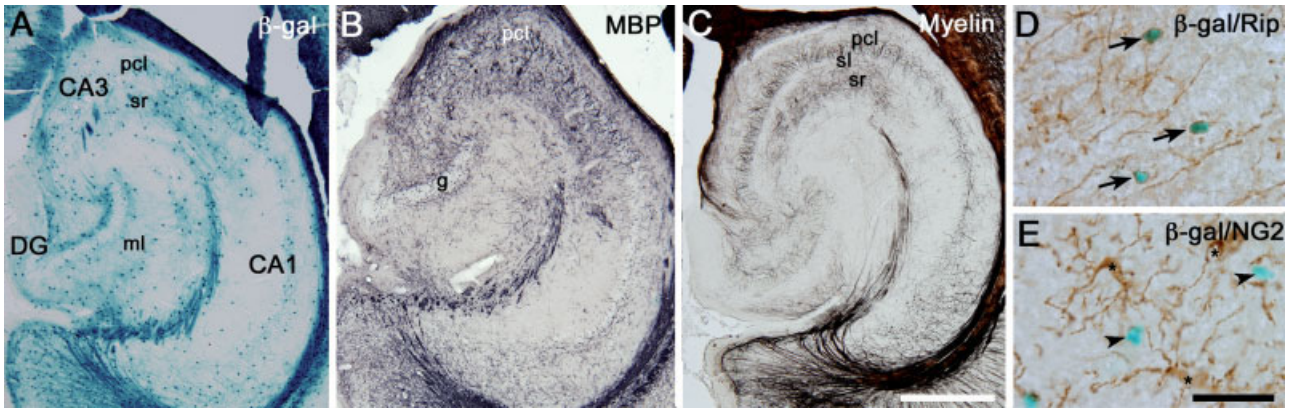


Fig. 3. Myelination pattern and LacZ transgene expression in the MBP-LacZ tg mouse. (**A**) Tissue section obtained from an unlesioned MBP-LacZ-tg mouse and enzymatically reacted for β-gal. Deposition of the blue reaction product is confined to myelin and oligodendrocytes. A relatively dense staining is seen in the stratum radiatum CA3. Myelinated PP fibres are seen in the molecular layer of the DG. (**B**) Immunohistochemical staining showing co-localization of MBP to the β-gal stained myelinated fibre tracts. (**C**) Silver impregnation showing the same distribution of myelin fibres as observed in (A) and (B). (**D**) Double labeling for $\beta\text{-gal}^+$ and $Rip^+$ identifying the $\beta\text{-gal}^+$ cells (arrows) as mature oligodendrocytes. Rip antigen is located to the plasmamembrane of oligodendrocytes and is observed as a brown rim around the blue $\beta\text{-gal}^+$ cell. (**E**) Double labeling showing absence of co-localization of β-gal (arrowheads) to $NG2^+$ cells (asterisks). CA1, regio superior hippocampus; CA3, regio inferior hippocampus; DG, dentate gyrus; g, granule cell layer; ml, molecular layer; pcl, pyramidal cell layer; sl, stratum lucidum; sr, stratum radiatum. Scale bars: 400 μm (A–C) and 30 μm (D,E). [Color figure can be viewed in the online issue, which is available at www.interscience.wiley.com.]

tated by correlation with the parallel toluidine blue stained sections (see Fig. 2). The sampling was initiated with a random initiation point. Counting was performed by the same person (N. Drøjdahl) in the right hippocampus of PP lesioned mice and unlesioned controls.

*Estimation of total fibre length by global spatial sampling.* The total length of myelinated axons was estimated in the srl-CA3 in parallel myelin silver stained sections from the MBP-LacZ tg mice. Total fibre length was estimated by global spatial sampling, by counting intersections of fibres with isotropically oriented virtual planes within a virtual box in a thick section with arbitrary orientation (Larsen et al., 1998). Due to difficulties in distinguishing the transition between CA3 and CA2 in the stained sections, the stratum radiatum CA2 was included in the srl-CA3. In addition during counting the srl-CA3 was split into (1) a deep fibre dense part superficial to the pyramidal cell layer, and (2) a superficial less fibre dense part subjacent to the deafferented molecular layer of the CA3. The total fibre length, $L$, of the region was estimated according to Larsen et al. (1998): $L = 1/\text{hsf} \times 1/\text{asf} \times 1/\text{ssf} \times d \times 2 \times \Sigma Q$, where d is the plane separation distance and Q is the counted fibre-plane intersections (hsf, ssf, and asf: see above). Every 16th section was selected for counting giving 6–7 sections with the srl-CA3. Counting was performed within a box, with a height of 10 μm (mean section thickness 14.9 μm ± 1.5 μm, 2 μm guard zone in the top, and a 2–3 μm guard zone in the bottom), a frame area (box) of 129 $\mu m^2$, and a plane separation distance, $d$, of 9.35 μm. Counting was performed at 2 different step lengths for the two sub-regions ($dx$, $dy$ (deep) = 150 μm × 150 μm and $dx$, $dy$ (superficial) = 80.3 μm × 80.3 μm). The total fibre length of the srl-CA3 was the sum of the total fibre length of the 2 sub-regions. Using, this method for length estimation the results should only be affected by the shrinkage of the fibres itself which is comparable between groups.

*Estimation of oligodendrocyte numbers.* The total number of oligodendrocytes was estimated by systematic random sampling in tissue sections from the MBP-LacZ tg mice. Using an approximation of the fractionater design by Gundersen and Jensen (1987) and West et al. (1991), cells were systematic randomly sampled along the entire septohippocampal axis of the srl-CA3. As done for the length estimation, the stratum radiatum CA2 was included in the srl-CA3. The total number of cells, $N$, were estimated by $N = \Sigma\ Q^- \times 1/\text{hsf} \times 1/\text{asf} \times 1/\text{ssf}$, where $Q^-$ is the number of cells counted, hsf is the height sampling fraction (height of disector/section thickness), asf is the area sampling fraction (area (frame)/area ($dx \times dy$ steps) and ssf is the section sampling fraction (Dorph-Petersen et al., 2001; West et al., 1991). Staining-induced tissue shrinkage in the z-axis prevented placement of a virtual counting box within the tissue section, the optical disector, and cells were instead counted through the entire height (15.3 μm ± 1.5 μm) of the section (1/tsf = 1). Total oligodendrocyte numbers might therefore be slightly underestimated due to loss of nuclei ("caps") from the cut surfaces of the sections (Andersen and Gundersen, 1999). With a random start, every 8th section was selected for quantification giving 11–14 sections with CA3 in each animal. The aim was to count around 150–300 cells per animal using a sampling frame of 2655 $\mu m^2$ and sampling steps of 90 μm × 90 μm ($dx$ ($dy$).

*Cavalieri volume estimation.* The sampling areas were used to estimate the reference volumes (Gundersen and Jensen, 1987), and were determined by exact delineation of the srl-CA3.

## G-ratio estimation

Axonal caliber and myelin thickness were measured on EM microphotographs of srl-CA3. The cross-sectional

axonal area of myelinated axons was measured and axonal caliber was determined by the diameter of a circle of area equivalent to each axon. The G-ratio was determined by dividing the diameter of the axon by the diameter of the fiber (axon with myelin). Measurements were performed with ImageJ.

### Quantification of BrdU-incorporating cells

Counting of $NG2^+$, $BrdU^+$, $BrdU^+NG2^+$, $\beta\text{-gal}^+$, and $BrdU^+\beta\text{-gal}^+$ cells 7 days after lesion was performed as described in Nielsen et al. (2006) in 10 parallel sections 160 μm apart, using a counting frame of 4900 μm (fraction of total area 61%) along the septohippocampal axis of the srl-CA3 starting 1900 μm from the surface of the brain. In animals with 9 weeks survival counting of $BrdU^+$, $\beta\text{-gal}^+$, and $BrdU^+\beta\text{-gal}^+$ was performed in 6 sections 300 μm apart using the same counting criteria as above. Results are based on counting of at least 150–200 single labeled $NG2^+$ or $\beta\text{-gal}^+$ cells pr animal.

### Statistics

To evaluate the precision of individual and group estimates (Gundersen and Osterby, 1981; Gundersen et al., 1999; Larsen et al., 1998; Wirenfeldt et al., 2003), the coefficient of errors (CEs) of the individual estimates and coefficient of variation (CV = standard deviation/mean) of the group were calculated. Results are given as mean ± SD and analyzed using non-parametric statistics. $P$ values are indicated as follows: $P < 0.05$: *, $P < 0.01$: **, and $P < 0.001$: ***.

## RESULTS

### β-Gal Expression in MBP-LacZ Transgenic Mice Co-Localizes to Myelinated Tracts and Oligodendrocytes

To validate the MBP-LacZ tg mice as suitable for studies of myelin and myelinating cells stainings for β-gal were compared to the staining for MBP and the myelin silver staining. Staining localized to the same subregions, including the srl-CA3 (Fig. 3A–C). The stainings also confirmed previous observations of myelination of the CA3-associated fibres in stratum radiatum (Berger and Frotscher, 1994; Drøjdahl et al., 2002), whereas the mossy fibres in stratum lucidum were unmyelinated (Fig. 3C) (Blackstad and Kjaerheim, 1961). Furthermore, co-localization of the oligodendrocyte and myelin marker Rip and β-gal to the same cells (Fig. 3D) confirmed that β-gal was expressed in oligodendrocytes in the MBP-LacZ tg mice. At the same time, there was no overlap in cellular expression of $\beta\text{-gal}^+$ and NG2 (Fig. 3E), emphasizing that only oligodendrocytes expressed β-gal.

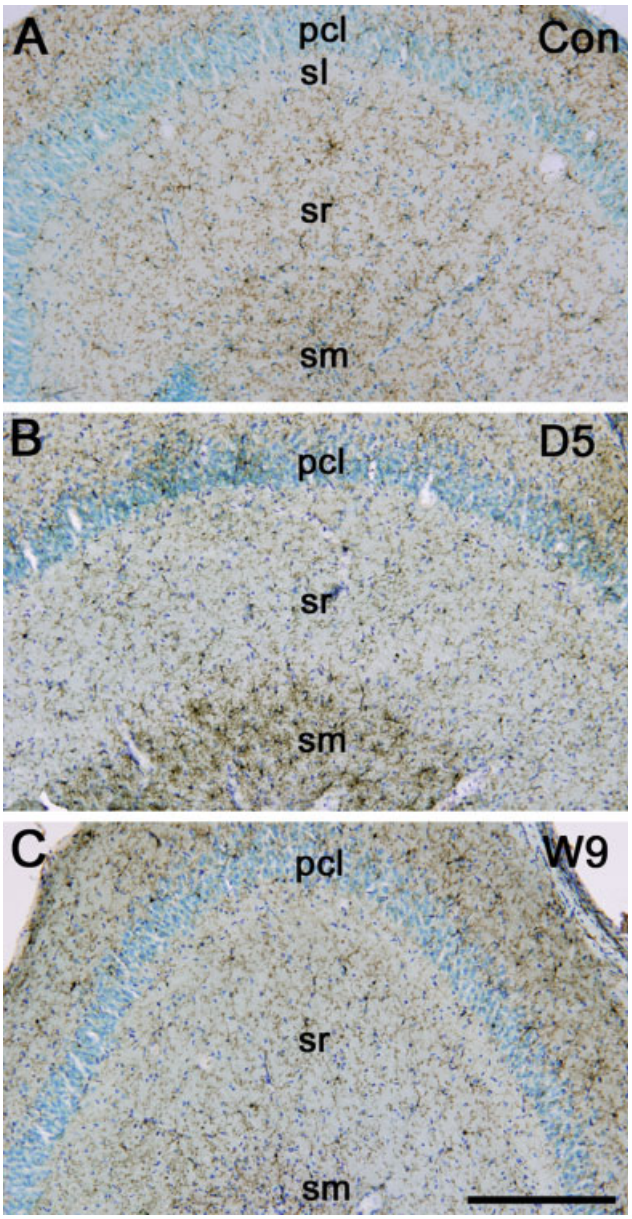


Fig. 4. Microglial response to PP lesion. CD11b staining of sections obtained from unlesioned control mouse (**A**), and PP lesioned mice 5 days (**B**) and 9 weeks (**C**) post lesion. At day 5 changes in the CA3 were clearly observed in the deafferented stratum moleculare (sm), whereas microglial CD11b staining in the srl-CA3 appeared unaffected. pcl, pyramidal cell layer; sl, stratum lucidum; sm, stratum moleculare; sr, stratum radiatum. Con, unlesioned control; D5, day 5 after PP lesion; W9, 9 weeks after PP lesion. Scale bar: 100 μm. [Color figure can be viewed in the online issue, which is available at www.interscience.wiley.com.]

### Axonal Transection Induces a Strong Microglial Response in Stratum Moleculare CA3 But Not in srl-CA3

Transection of the PP in the entorhinal cortex results in a dense anterograde axonal and terminal degeneration and lesion-induced microglial activation in its field of termination in the CA3 (Jensen et al., 1999; Matthews et al., 1976). This was reflected in increased

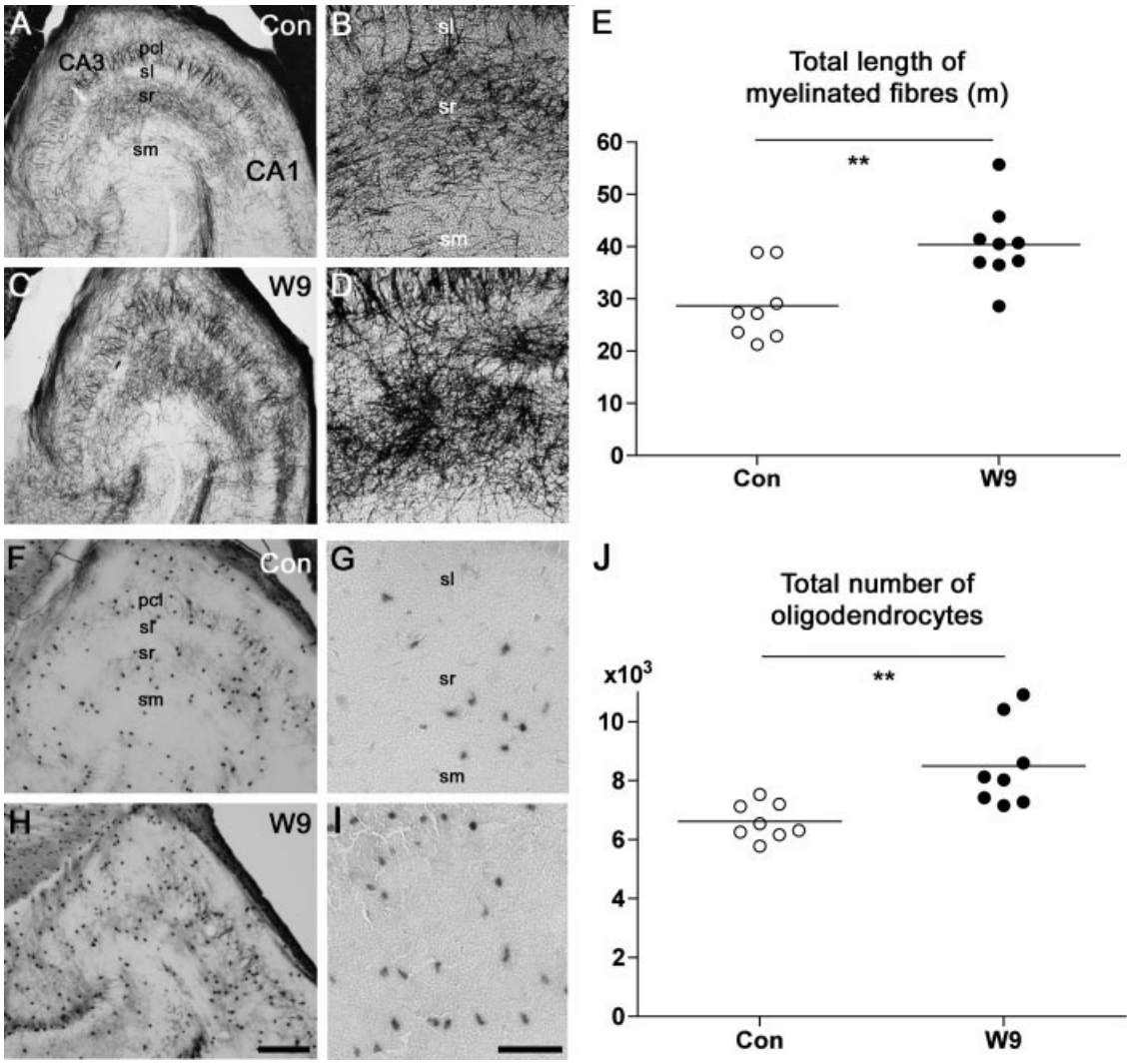


Fig. 5. Sprouting-associated increase of the total length of silver impregnated myelinated fibres and number of β-gal$^+$ oligodendrocytes in the srl-CA3. (**A–D**) Sections used for the quantification of myelin fibre length in the srl-CA3 from an unlesioned mouse (A, B) and a lesioned mouse 9 weeks post lesion (C, D). (B, D) show high magnifications from (A, C). An increased density of fibres was observed in the deep layers of stratum radiatum 9 weeks post lesion. (**E**) Stereological quantification shows a marked 41% increase in the length of myelinated fibres in the srl-CA3 9 weeks post lesion. For additional information see Table 1. (**F–I**) β-gal$^+$ oligodendrocytes in srl-CA3 of unlesioned mice (F, G) and PP-lesioned mice 9 weeks post lesion (H, I). (G, I) High power photomicrographs from (F, G). Compared to unlesioned mice, the number and β-gal expression of oligodendrocytes in the srl-CA3 was increased after 9 weeks (H, I). (**J**) Quantification showed a significant 28% increase in the total number of β-gal$^+$ oligodendrocytes 9 weeks post lesion. Additional data are given in Table 2. CA1, regio superior hippocampus; CA3, regio inferior hippocampus; pcl, pyramidal cell layer; sl, stratum lucidum; sm, stratum moleculare; sr, stratum radiatum. ** $P < 0.01$; Con, unlesioned control; W9, 9 weeks after PP lesion. Scale bars: 200 μm (A, C, E, H) and 20 μm (B, D, G, I).

*TABLE 1. Total Length of Myelinated Fibres in the srl-CA3*

| | Region, srl-CA3 | Number of mice ($n$) | Total myelin fibre length (m): mean (CE) | CV | Total volume (mm$^3$): mean ± SD |
|---|---|---|---|---|---|
| Control | Total | 8 | 28.7 | 0.24 | 0.85 ± 0.11 |
| | Deep | | 24.9 (0.07) | 0.26 | 0.65 ± 0.11 |
| | Superficial | | 3.8 (0.09) | 0.26 | 0.20 ± 0.02 |
| 9 weeks | Total | 9 | 40.4** | 0.18 | 0.87 ± 0.08 |
| | Deep | | 35.9 (0.05)** | 0.18 | 0.67 ± 0.07 |
| | Superficial | | 4.5 (0.08) | 0.23 | 0.20 ± 0.03 |

**$P < 0.01$ compared to unlesioned control.

microglial CD11b staining in the deafferented stratum moleculare CA3 5 days after lesion (Fig. 4A,B). The microglial reaction had vanished 9 weeks after lesion (Fig. 4C). In contrast to the microglial response in stratum moleculare CA3, PP lesion did not elicit a visible microglial reaction in the srl-CA3 at neither 5 days nor 9 weeks (Fig. 4B,C). This was in accordance with previous observations of absence of silver stained degenerat-

ing nerve fibres and terminals in the srl-CA3 (Drøjdahl et al., 2002; Jensen et al., 1999, 2000a).

### Sprouting of CA3-Associated Fibres is Reflected in Increased Total Length of Silver Stained Myelinated Fibres

To investigate if axonal lesion-induced sprouting in the CA3 (Drøjdahl et al., 2002; Jensen et al., 2000b; Zimmer et al., 1974) also included the myelinated CA3-associated fibres, the silver stained material from mice with 9 weeks survival post lesion was analyzed. We observed an increased density of silver stained fibres, most pronounced in the deep fibre dense part of stratum radiatum CA3 (Fig. 5A–D). To avoid bias from shrinkage or expansion induced to the srl-CA3 due to lesion or tissue processing we used stereology for estimation and subsequent comparison of the total length of myelinated fibres in the srl-CA3 from lesioned and unlesioned mice (Fig. 5E and Table 1). Nine weeks after lesion the total length of myelinated fibres had increased 41% ($P < 0.01$) in the srl-CA3 of lesioned compared to unlesioned mice, most pronounced in the deep part of CA3 (Table 1). CEs of individual estimates were 5–8% and CV's of the group means were 18%–26% (Table 1). The change in fibre length was not due to variation in the delineation of the regions as the estimates of the volumes were similar in the 2 groups (Table 1).

*TABLE 2. Number of β-Galactosidase$^+$ Oligodendrocytes in the srl-CA3*

| srl-CA3 | Number of mice ($n$) | Number of β-galactosidase$^+$ oligodendrocytes: mean (CE) | CV | Total volume ($mm^3$): mean ± SD |
|---|---|---|---|---|
| Control | 8 | 6610 (0.06) | 0.09 | 0.77 ± 0.07 |
| 5 days | 7 | 5760 (0.07) | 0.18 | 0.70 ± 0.04 |
| 9 weeks | 8 | 8490 (0.06)** | 0.17 | 0.77 ± 0.07 |
| Sham | 4 | 4800 (0.07) | 0.15 | 0.67 ± 0.06 |

**$P < 0.01$ compared to unlesioned control.

### Increased Total Length of Myelinated of Fibres Is Associated with Increased Numbers of Oligodendrocytes

Next, the response of β-gal$^+$ oligodendrocytes to PP lesion was analyzed. There were no visible changes of

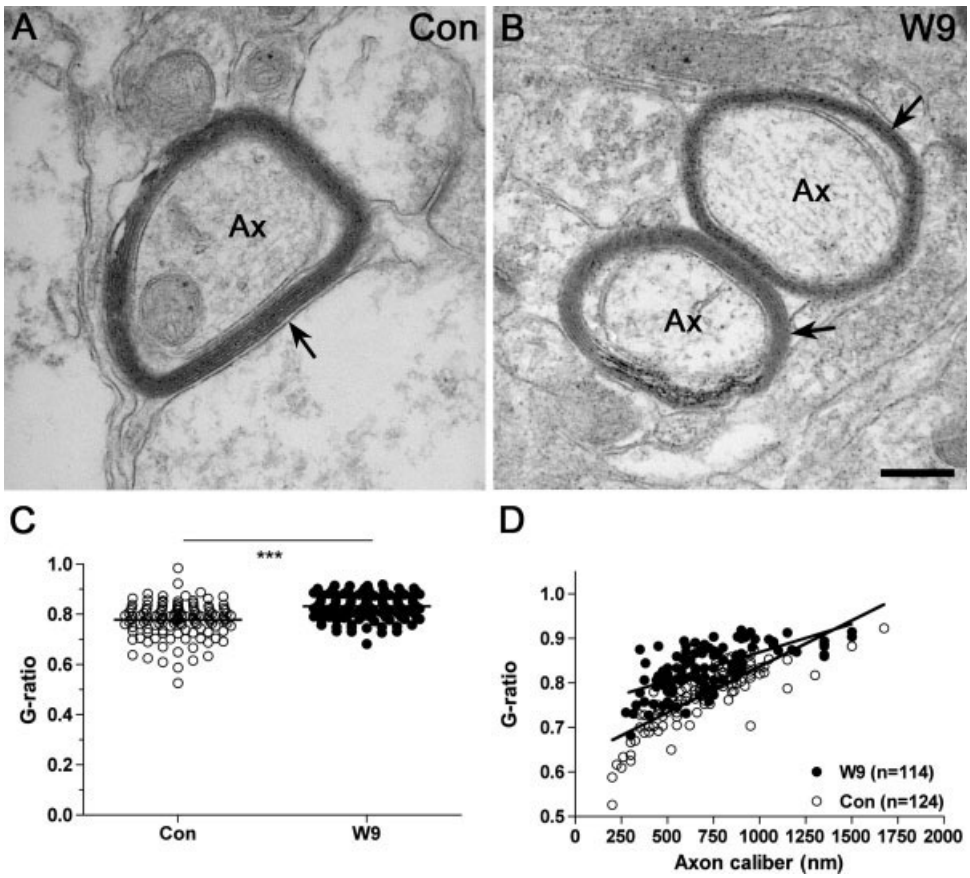


Fig. 6. Myelin thickness of sprouting and preexisting CA3-associated fibres. (**A**, **B**) Electron microscopy microphotographs obtained from srl-CA3 showing the myelin sheath (arrow) of an axon (ax) from an unlesioned control (A) and a PP lesioned mouse (B), 9 weeks after lesion. Note the decrease in the number of lamellae in the lesioned mouse, although the axon caliber is unchanged. (**C**, **D**) Estimations of G-ratio of the fibres in the srl-CA3 of lesioned mice ($n = 3$) compared to unlesioned controls ($n = 2$). Comparison of the mean G-ratio showed a larger G-ratio in lesioned mice compared to unlesioned controls (C). The G-ratio in relation to axonal calibre (D) illustrates the difference in G-ratios although the mean axon calibre was comparable. Arrows indicate the myelin sheath. Ax, axon; Con, unlesioned control; W9, 9 weeks after PP lesion *** $P < 0.001$. Scale bar: 200 nm (A, B).

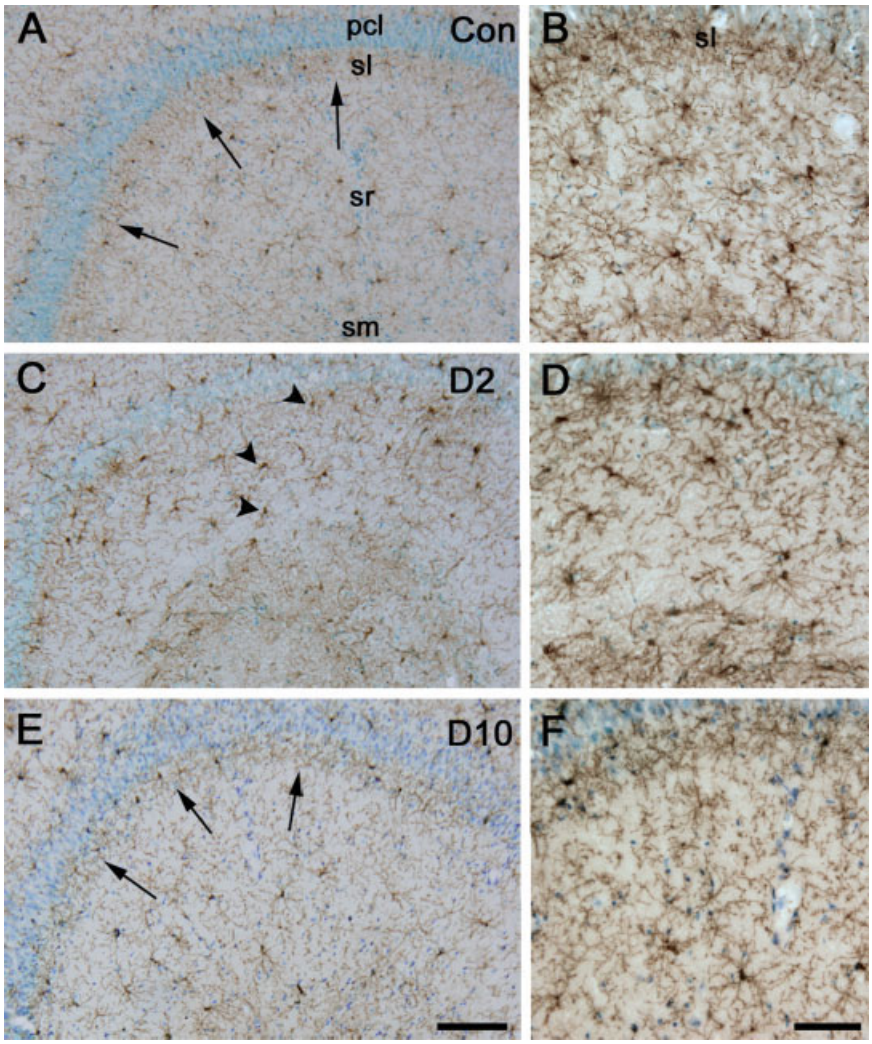


Fig. 7. Lesion-induced changes of $NG2^+$ cells in the srl-CA3. High power photomicrographs from (**A**, **D**, **E**) are shown in the column to the right (**B**, **D**, **F**). (**A**, **B**) In unlesioned mice (A), the $NG2^+$ cells are arborized and evenly distributed throughout the CA3. Organization of cellular processes is different in the stratum lucidum, which makes this zone appear more intensily stained (arrows). (C–F) Lesion results in a transient disintegration of the zone of $NG2^+$ cells in stratum lucidum and transient morphological changes of $NG2^+$ cells in stratum radiatum at day 2 (C, D). The zone reappears from days 7–10 (E, F) and remains at 9 weeks (not shown). pcl, pyramidal cell layer; sl, stratum lucidum; sm, stratum moleculare; sr, stratum radiatum. Con, unlesioned control; D2, 2 days after PP lesion; W9, 9 weeks after PP lesion. Scale bar: 200 μm (A, C, E) and 20 μm (B, D, F). [Color figure can be viewed in the online issue, which is available at www.interscience.wiley.com.]

the $\beta$-gal$^+$ cells in the srl-CA3 5 days after lesion, but at 9 weeks the density of oligodendrocytes and the staining intensity of the neuropil in the srl-CA3 had increased (Fig. 5F–I). This observation was confirmed through quantification of $\beta$-gal$^+$ oligodendrocytes (Fig. 5J and Table 2) that showed a 28% increase in the number of oligodendrocytes in the srl-CA3 of lesioned compared to unlesioned mice at 9 weeks ($P < 0.05$), but no changes in the total number of oligodendrocytes 5 days after lesion or following sham-surgery (Table 2). The CEs of the individual estimates of the $\beta$-gal$^+$ oligodendrocytes were 6–8%, with CV values of 7–23% of the estimated mean values (Table 2). Volumetric analysis of the srl-CA3 showed no lesion-induced changes (Table 2). This emphasized that the observed increase of oligodendrocytes in the srl-CA3 was not due to different delineation at quantification.

## Myelin Thickness of Sprouting and Preexisting CA3-Associated Fibres

We next asked if the sprouting axons developed thin myelin, as in remyelination (Blakemore, 1974; Ludwin and Maitland, 1984), or if they developed thick myelin within the 9 weeks observation period. In order to answer this question we investigated by electron microscopy the caliber of transversally cut srl-CA3 fibres and axons from lesioned and unlesioned mice. The mean axon diameter in unlesioned mice was 704.4 nm ± 259.8 (124 fibres) and was thereby in the same range as in lesioned mice 710.2 nm ± 252.7 (114 fibres). In comparison, the mean number of myelin lamellae was smaller in lesioned mice 4.3 ± 1.1 (105 fibres) as compared to unlesioned mice 6.2 ± 1.4 (122 fibres) ($P < 0.0001$) (Fig. 6A,B and data not shown). This was also reflected in that the fibres in the srl-CA3 of

lesioned mice had a larger G-ratio (0.83 ± 0.05) than unlesioned mice (0.78 ± 0.07) ($P < 0.0001$) (Fig. 6C,D). Taken together, these results indicated that the sprouting fibers had obtained their final caliber, whereas the myelination of the sprouting fibers remained incomplete 9 weeks after lesion.

### Sprouting of CA3-Associated Fibres Results in Formation of New Oligodendrocytes

To determine whether the increased number of β-gal$^+$ oligodendrocytes might be generated from adult oligodendrocyte precursor cells we studied the lesion-response of the NG2$^+$ cells in the srl-CA3. In normal mice, the process-bearing NG2$^+$ cells were evenly distributed in stratum radiatum CA3, while they were more intensely stained and densely packed in stratum lucidum CA3 (Fig. 7A,B). Two days after lesion, the NG2$^+$ cells became slightly hypertrophic and their cell processes in stratum lucidum were re-arranged, erasing the border to stratum radiatum (Fig. 7C,D). The border between stratum lucidum and stratum radiatum reappeared through days 7–10 (Fig. 7E,F) when the NG2$^+$ cells had normalized their morphology throughout CA3.

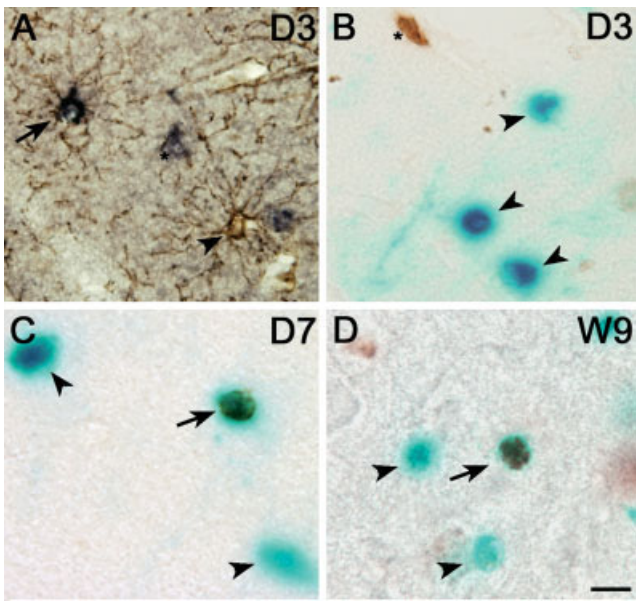


Fig. 8. Lesion-induced proliferation of oligodendrocyte lineage cells in the srl-CA3. (**A**) Double labeling for BrdU$^+$ (bluish black) and NG2$^+$ (brown) showing a double labeled BrdU$^+$NG2$^+$ cell (arrow) day 3 suggestive of proliferation. Note also a BrdU$^-$NG2$^+$ cell (arrowhead) and a BrdU$^+$NG2$^-$ cell (*) in the same visual field. (**B**, **C**) BrdU$^-$β-gal$^+$ cells (arrowheads) 3 days (B), 7 days (C), and 9 weeks (**D**) after lesion. Although several BrdU$^+$ cells (*) were observed 3 days after lesion (B), double-labeled BrdU$^+$β-gal$^+$ cells (arrow) were not observed until 7 days after lesion (C), when they were observed along with BrdU$^-$β-gal$^+$ (arrowheads). (**D**) BrdU$^+$β-gal$^+$ cells were also observed 9 weeks after lesion, showing that these newly formed cells were long-lived. D3, 3 days after lesion; D7, 7 days after lesion; W9, 9 weeks after lesion. Scale bar: 10 μm. [Color figure can be viewed in the online issue, which is available at www.interscience.wiley.com.]

We have previously shown that PP lesion results in morphological changes and proliferation of NG2$^+$ cells and in formation of new oligodendrocytes in the dentate gyrus (Nielsen et al., 2006). To investigate the origin of the lesion-induced increase in the number of oligodendrocytes in the srl-CA3, PP-lesioned mice were injected with BrdU with 8-h intervals from 24 to 72 h and killed 7 days after lesion. Quantification of the number of NG2$^+$, BrdU$^+$, and BrdU$^+$NG2$^+$ cells in sections double stained for BrdU and NG2, showed that lesion resulted in BrdU-incorporation into 21% of NG2$^+$ cells in the srl-CA3 of the ipsilateral hippocampus (Fig. 8A), which was significantly more than in the unlesioned, contralateral srl-CA3, where 4% of NG2$^+$ cells had incorporated BrdU ($P < 0.01$, $n = 7$; data not shown). Furthermore, quantification of β-gal$^+$, BrdU$^+$, and BrdU$^+$β-gal$^+$ cells in double stained adjacent sections showed that 5% of β-gal$^+$ oligodendrocytes in the ipsilateral srl-CA3 had been generated through proliferation (Fig. 6B), as opposed to 0.3% of oligodendrocytes in the contralateral srl-CA3 ($P < 0.01$, $n = 7$; data not shown).

Next, to determine if the BrdU$^+$β-gal$^+$ cells that were observed 7 days after lesion, oligodendrocytes, arose from oligodendrocytes that had become labeled during the BrdU injection interval or from differentiation of proliferating NG2$^+$ cells, additional groups of mice were subjected to BrdU injections 48–72 h after lesion and terminated either 1 h or 9 weeks after the last injection. Quantification showed that 2.5% ± 0.5% of β-gal$^+$ oligodendrocytes in the ipsilateral srl-CA3 of animals, which had survived for 9 weeks, had incorporated BrdU, compared to 0% in the contralateral srl-CA3 (Fig. 8C, Table 3, $P < 0.01$). This was also significantly higher than the number of BrdU$^+$β-gal$^+$ oligodendrocytes in the srl-CA3 (2.5% ± 0.5% vs 0.5% ± 0.5%; $P < 0,01$) of animals with similar period of BrdU-incorporation but terminated 1 h after the last BrdU injection 3 days after lesion (Table 3). In combination with the observation that 11% of the

*TABLE 3. Percentage of Double Labeled Proliferating Cells in the srl-CA3*

| | % BrdU-incorporating cells | | | |
|---|---|---|---|---|
| | Survival: 3 days; number of mice, $n = 7$ | | Survival: 9 weeks; number of mice, $n = 6$ | |
| Cell type | Contralateral, mean ± SD | Ipsilateral, mean ± SD | Contralateral, mean ± SD | Ipsilateral, mean ± SD |
| BrdU$^+$NG2$^+$ cells | 1.1 ± 0.4 | 11.3 ± 2.3$^{***}$ | – | – |
| BrdU$^+$βgal$^+$ cells | 0.3 ± 0.5 | 0.5 ± 0.5 | 0.0 ± 0.1 | 2.5 ± 0.5$^{**,(**)}$ |

$^{**}P < 0.01$ and $^{***}P < 0.001$ compared to the contralateral values; $^{(**)}P < 0.01$ compared to the value for the ipsilateral srl-CA3, 3 days post lesion.

$NG2^+$ cells in the ipsilateral srl-CA3 had incorporated BrdU (Table 3), this suggested that the $BrdU^+\beta\text{-gal}^+$ oligodendrocytes that were present in the srl-CA3 9 weeks after lesion had been generated by differentiation of $NG2^+$ cells incorporating BrdU from 48–72 h post-lesion, and not from proliferation of pre-existing oligodendrocytes. The data also showed that these newly generated oligodendrocytes were long-lived compatible with the increased total length of myelinated fibres 9 weeks after lesion.

## DISCUSSION

This is, to our knowledge, the first study that provides estimates of changes in oligodendrocyte numbers and length of myelinated fibres induced by axonal sprouting in the adult CNS. The results of the study show that oligodendrocyte lineage cells retain their capacity to engage in myelination processes in the adult CNS provided that they are adequately stimulated by axons. Using stereological methods, we report that axonal lesion-induced sprouting in the hippocampal srl-CA3 (Drøjdahl et al., 2002; 2004; Zimmer, 1974) results in a marked 41% increase in the total length of myelinated fibres, and that these fibres show the same fibre diameter, but thinner than normal myelin thickness, 9 weeks after lesion. Importantly, the increase in myelinated fibres was accompanied by a 28% increase in the number of oligodendrocytes, with sequential appearance of newly formed $NG2^+$ cells and thereafter oligodendrocytes in the srl-CA3. These changes might even be underestimated since cells were quantified along the entire hippocampal axis, while the PP fibres in the most septal and temporal parts were unlikely to be transected by the present single wire-knife cut.

The significant lesion-induced increase in the total length of myelinated CA3-associated fibres provides evidence of a considerable plasticity of myelinated fibres, and shows that the axon is a strong regulator of oligodendrocyte recruitment and myelination in adult CNS. The CA3 pyramidal cells give rise to three main classes of connections; the longitudinal associational path that extends within stratum radiatum CA3 where it connects different segments of CA3, the Schaffer collaterals projecting from CA3 to stratum radiatum CA1, and the commissural connections to the contralateral hippocampus (Amaral and Witter, 1995; Blackstad, 1956). In order words, the main afferent input to stratum radiatum CA3 originates from the CA3 pyramidal cells themselves. Furthermore, the cholinergic afferents to the hippocampus are unmyelinated (Frotscher and Leranth, 1985). Taken together, this means that the majority of the newly formed myelinated fibres must arise from intact axons from the ipsi- or contralateral CA3 pyramidal cells that are induced to sprout within the srl-CA3. High expression of growth associated proteins, such as growth-associated-protein-43 (GAP-43), by the CA3 pyramidal cells, is in line with a high growth potential of these cells (Himi et al., 1994; Kruger et al., 1992).

The NG2 cell response within the srl-CA3 consisted of transient morphological changes, in the form of a moderate hypertrophy of the cell bodies and a changed orientation of their processes that ablated the otherwise normal border between the stratum radiatum and stratum lucidum CA3. The morphological changes of the $NG2^+$ cells in stratum lucidum can perhaps be ascribed to, that the CA3 pyramidal cells, in addition to deafferentation of the distal segment of their apical dendrites, were subjected to transsynaptic changes at the base of their apical dendrites in the stratum lucidum (Helme-Guizon et al., 1998), due to the deafferentation of the dentate granule cells (Blackstad and Kjaerheim, 1961). Although the morphological changes of the $NG2^+$ cells were not as marked as observed in the PP-deafferented dentate gyrus (Dehn et al., 2005; Nielsen et al., 2006), the incorporation of BrdU into 21% of $NG2^+$ cells in the srl-CA3 was comparable to the proliferative response in the molecular layer of the dentate gyrus 7 days after PP lesion (Nielsen et al., 2006). Taken together with the observation of normal numbers of oligodendrocytes in the srl-CA3 5 days after lesion, and the significantly increased numbers of oligodendrocytes, of which some had incorporated BrdU, 9 weeks after lesion, this suggested that the $NG2^+$ cells had received a very strong stimulus, with differentation of a small proportion of $NG2^+$ cells into oligodendrocytes days to weeks after lesion. The time course of the injury-induced axonal sprouting in srl-CA3 has not yet been established, but it is likely that it would be as described for the PP deafferented rat dentate gyrus where axonal elongation has been reported to begin 4-6 days after lesion, and to be almost complete 12 days after lesion (Steward and Vinsant, 1983).

The observation of a 41% increase in the total length of myelinated fibres in the srl-CA3, and a 28% increase in the number of oligodendrocytes, raises questions about (1) which cells, newly formed oligodendrocytes, or a mixture of newly formed and preexisting oligodendrocytes, form the new myelin, and (2) the properties of the newly formed myelin in term of myelin sheath thickness and internode length, compared to the pre-existing myelin. The estimation of fibre length and number of oligodendrocytes in the srl-CA3 of both lesioned and unlesioned mice allowed calculation of the average internode length per oligodendrocyte. Calculations showed that the average amount of myelin produced per oligodendrocyte in srl-CA3 of unlesioned mice was 4.3 mm myelin/oligodendrocyte (28.7 m myelin/6,610 oligodendrocytes), which was within the range reported for the rat fimbria, which encompasses the CA3 commissural fibres. In this structure, Suzuki and Raisman (1992) observed 20–40 internodes about 150–250 μm long per oligodendrocyte, summing up to a total production of 3.0–10.0 μm of myelin per oligodendrocyte. If all oligodendrocytes contributed equally to myelinate preexisting and added fibres in the srl-CA3, 9 weeks after lesion, the total production of myelin would accordingly increase from 4.3 to 4.8 mm myelin/oligodendrocyte (40.4 m myelin/8,490 oligodendrocytes). In comparison, if the sprouting fibres were myelinated exclusively by newly formed oligodendro-

cytes these oligodendrocytes should produce 6.2 mm myelin/oligodendrocyte (11.7 m myelin/1,880 oligodendrocytes). Since we in both situations speak about increased myelin elaboration per oligodendrocyte, this might in itself explain the thinner myelin sheaths and thus the increased G-ratio of the myelinated fibres in the srl-CA3 of lesioned mice 9 weeks after surgery. It is intriguing that increased G-ratio is also a feature of myelin generated during remyelination of demyelinated fibres (Ludwin and Maitland, 1984). However, since the post lesion survival time was only 9 weeks, our observation of an increased G-ratio might also reflect that the myelination process was still ongoing.

In line with the induction of morphological changes of the $NG2^+$ cells in the srl-CA3, PP lesion has been previously shown to induce a moderate microglial and astroglial reaction in the same layers (Hailer et al., 1999). However, this response was by far exceeded by the microglial reaction in the deafferented stratum moleculare CA3 (Hailer et al., 1999), and it could not be clearly discerned in our material. Similar to the lesion-dependent differences in micro- and astroglial response in the stratum moleculare CA3 and the srl-CA3, induction of glial-derived cytokines and growth factors following PP lesion has been shown to be largely confined to the deafferented stratum moleculare CA3, whereas induction is limited in the non-deafferented srl-CA3 (Gomez-Pinilla et al., 1992; Guthrie et al., 1995; Jensen et al., 2000a). This regional segregation supports the view that sprouting axons, rather than lesion-induced cytokines and growth factors are responsible for the presently observed induction of oligodendrocyte formation and myelination. This was further substantiated by the timeprofile of the increase in oligodendrocyte numbers, which was first observed at 9 weeks, and not at 5 days or at earlier time points, when the lesion-induced synthesis of cytokines and growth factors in the deafferented stratum moleculare is highest (Fagan and Gage, 1990; Gomez-Pinilla et al., 1992; Guthrie et al., 1995; Jensen et al., 2000a).

Several studies have implicated axonal damage (Kuhlmann et al., 2002; Trapp et al., 1998), axolemmal changes (Sedgwick, 1997), and re-expression of developmentally expressed myelin-inhibitory proteins (Charles et al., 2002; Lee et al., 2007; Mi et al., 2005), in the demyelinating pathology in patients with multiple sclerosis and in experimental models of multiple sclerosis. Other studies have indicated that axonal surface membrane proteins, that are crucial to proper myelination during development (John and Key, 2003; Kim et al., 2003; Mihailov et al., 2004), may be induced or expressed at insufficient levels and thereby impact on remyelinating capacity of the oligodendroglial lineage under the same conditions. The presently obtained results point to signals elicited by the sprouting axon as possible means to enhance myelin repair in the adult CNS. Thus, elucidation of the molecular similarities and discrepancies between developing, sprouting, and demyelinated axons may facilitate the development of new strategies to improve myelin regeneration.

## ACKNOWLEDGMENTS

The expert technical assistance provided by Lene Jørgensen, Susanne Petersen (Medical Biotechnology Centre, University of Southern Denmark), Inger Margrethe Rasmussen and Anni Petersen (Anatomy and Neurobiology, University of Southern Denmark), Frauke Winzer (Anatomy, University Rostock), Priscilla Valera and Margaret Attiwell, McGill University Health Care Centre, and the Service Commun d'Imagerie et d'Analyses Microscopiques de l'Université d'Angers is gratefully acknowledged.

## REFERENCES

Amaral DG, Witter MP. 1995. Hippocampal formation. In: Paxinos G, editor. The rat nervous system, 2nd ed. San Diego: Academic Press. pp 443–485.

Andersen BB, Gundersen HJ. 1999. Pronounced loss of cell nuclei and anisotropic deformation of thick sections. J Microsc 196:69–73.

Bansal R, Pheiffer SE. 1985. Developmental expression of 2′, 3′-cyclic nucleotide 3′-phosphohydrolase in dissociated fetal rat brain cultures and rat brain. J Neurosci Res 14:21–34.

Barres BA, Raff MC. 1993. Proliferation of oligodendrocyte precursor cells depends on electrical activity in axons. Nature 361:258–260.

Baumann N, Pham-Dinh D. 2001. Biology of oligodendrocyte and myelin in the mammalian central nervous system. Physiol Rev 81:871–927.

Benes FM, Turtle M, Khan Y, Farol P. 1994. Myelination of a key relay zone in the hippocampal formation occurs in the human brain during childhood, adolescence, and adulthood. Arch Gen Psychiatry 51:477–484.

Bengtsson SL, Nagy Z, Skare S. Forsman L, Forssberg H, Ullén F. 2005. Extensive piano practicing has regionally specific effects on white matter development. Nat Neurosci 8:1148–1150.

Berger T, Frotscher M. 1994. Distribution and morphological characteristics of oligodendrocytes in the rat hippocampus in situ and in vitro: An immunocytochemical study with the monoclonal Rip antibody. J Neurocytol 23:61–74.

Blakemore WF. 1974. Pattern of remyelination in the CNS. Nature 249(457):577–578.

Blackstad TW. 1956. Commisural connections of the hippocampal region in the rat, with special reference to their mode of termination. J Comp Neurol 105:417–537.

Blackstad TW, Kjaerheim Å. 1961. Special axo-dendritic synapses in the hippocampal cortex: Electron and light microscopic studies on the layer of mossy fibres. J Comp Neurol 117:133–159.

Burne JF, Staple JK, Raff MC. 1996. Glial cells are increased proportionally in transgenic optic nerves with increased numbers of axons. J Neurosci 16:2064–2073.

Butt AM, Berry M. 2000. Oligodendrocytes and the control of myelination in vivo: New insights from the rat anterior medullay velum. J Neurosci Res 59:477–488.

Carmichael ST, Wei L, Rovainen CM, Woolsey TA. 2001. New patterns of intracortical projections after focal cortical stroke. Neurobiol Dis 8:910–922.

Cellerino A, Carroll P, Thoenen H, Barde YA. 1997. Reduced size of retinal ganglion cell axons and hypomyelination in mice lacking brain-derived neurotrophic factor. Mol Cell Neurosci 9:397–408.

Charles P, Reynolds R, Seilhean D, Rougon G, Aigrot MS, Niezgoda A, Zalc B, Lubetzki C. 2002. Re-expression of PSA-NCAM by demyelinated axons: An inhibitor of remyelination in multiple sclerosis? Brain 125:1972–1979.

Dehn D, Burbach GJ, Schafer R, Deller T. 2006. NG2 upregulation in the denervated rat fascia dentata following unilateral entorhinal cortex lesion. Glia 53:491–500.

Deller T, Frotscher M. 1997. Lesion-induced plasticity of central neurons: Sprouting of single fibres in the rat hippocampus after unilateral entorhinal cortex lesion. Prog Neurobiol 53:687–727.

Demerens C, Stankoff B, Logak M, Anglade P, Allinquant B, Couraud F, Zalc B, Lubetzki C. 1996. Induction of myelination in the central nervous system by electrical activity. Proc Natl Acad Sci USA 93:9887–9892.

Dinocourt C, Gallagher SE, Thompson SM. 2006. Injury-induced axonal sprouting in the hippocampus is initiated by activation of trkB receptors. Eur J Neurosci 24:1857–1866.

Dissing-Olesen L, Ladeby R, Nielsen HH, Toft-Hansen H, Dalmau I, Finsen B. 2007. Axonal lesion-induced microglial proliferation and microglial cluster formation in the mouse. Neurosci 149:112–122.
Dorph-Petersen KA, Nyengaard JR, Gundersen HJ. 2001. Tissue shrinkage and unbiased stereological estimation of particle number and size. J Microsc 204:232–246.
Drøjdahl N, Hegelund IV, Poulsen FR, Wree A, Finsen B. 2002. Perforant path lesioning induces sprouting of CA3-associated fibre systems in mouse hippocampal formation. Exp Brain Res 144:79–87.
Drøjdahl N, Fenger C, Nielsen HH, Owens T, Finsen B. 2004. Dynamics of oligodendrocyte responses to anterograde axonal (Wallerian) and terminal degeneration in normal and TNF-transgenic mice. J Neurosci Res 75:203–217.
Fagan AM, Gage FH. 1990. Cholinergic sprouting in the hippocampus: A proposed role for IL-1. Exp Neurol 110:105–120.
Fanarraga ML, Griffiths IR, Zhao M, Duncan ID. 1998. Oligodendrocytes are not inherently programmed to myelinate a specific size of axon. J Comp Neurol 399:94–100.
Foran DR, Peterson AC. 1992. Myelin acquisition in the central nervous system of the mouse revealed by an MBP-Lac Z transgene. J Neurosci 12:4890–4897.
Franklin RJ. 2002. Why does remyelination fail in multiple sclerosis? Nat Rev Neurosci 3:705.
Friedman B, Hockfield S, Black JA, Woodruff KA, Waxman SG. 1989. In situ demonstration of mature oligodendrocytes and their processes: An immunocytochemical study with a new monoclonal antibody, rip. Glia 2:380–390.
Frotscher M, Leranth C. 1985. Cholinergic innervation of the rat hippocampus as revealed by choline acetyltransferase immunocytochemistry: A combined light and electron microscopic study. J Comp Neurol 239:237–46.
Gomez-Pinilla F, Lee JW, Cotman CW. 1992. Basic FGF in adult rat brain: Cellular distribution and response to entorhinal lesion and fimbria-fornix transection. J Neurosci 12:345–355.
Gundersen HJ. 1986. Stereology of arbitrary particles. A review of unbiased number and size estimators and the presentation of some new ones, in memory of William R. Thompson. J Microsc 143:3–45.
Gundersen HJ, Jensen EB. 1987. The efficiency of systematic sampling in stereology and its prediction. J Microsc 147:229–263.
Gundersen HJ, Jensen EB, Kieu K, Nielsen J. 1999. The efficiency of systematic sampling in stereology—reconsidered. J Microsc 193:199–211.
Gundersen HJ, Osterby R. 1981. Optimizing sampling efficiency of stereological studies in biology: Or "do more less well!" J Microsc 121:65–73.
Guthrie KM, Nguyen T, Gall CM. 1995. Insulin-like growth factor-1 mRNA is increased in deafferented hippocampus: Spatiotemporal correspondence of a trophic event with axon sprouting. 352:147–160.
Hailer NP, Grampp A, Nitsch R. 1999. Proliferation of microglia and astrocytes in the dentate gyrus following entorhinal cortex lesion: A quantitative bromodeoxyuridine-labelling study. Eur J Neurosci 11:3359–3364.
Helme-Guizon A, Davis S, Israel M, Lesbats B, Mallet J, Laroche S, Hicks A. 1998. Increase in syntaxin 1B and glutamate release in mossy fibre terminals following induction of LTP in the dentate gyrus: A candidate molecular mechanism underlying transsynaptic plasticity. Eur J Neurosci 10:2231–2237.
Himi T, Okazaki T, Mori N. 1994. SCG10 mRNA localization in the hippocampus: Comparison with other mRNAs encoding neuronal growth-associated proteins (nGAPs). Brain Res 655:177–185.
Jensen MB, Hegelund IV, Lomholt ND, Finsen B, Owens T. 2000a. IFN-gamma enhances microglial reactions to hippocampal axonal degeneration. J Neurosci 20:3612–3621.
Jensen MB, Hegelund IV, Poulsen FR, Owens T, Zimmer J, Finsen B. 1999. Microglial reactivity correlates to the density and the myelination of the anterogradely degenerating axons and terminals following perforant path denervation of the mouse fascia dentata. Neurosci 93:507–518.
Jensen MB, Poulsen FR, Finsen B. 2000b. Axonal sprouting regulates myelin basic protein gene expression in denervated mouse hippocampus. Int J Dev Neurosci 18:221–235.
John JA, Key B. 2003. Axon mis-targeting in the olfactory bulb during regeneration of olfactory neuroepithelium. Chem Senses 28:773–779.
Kapfhammer JP. 1997. Axon sprouting in the spinal cord: Growth promoting and growth inhibitory mechanisms. Anat Embryol (Berl) 196:417–426.
Kim JY, Sun Q, Oglesbee M, Yoon SO. 2003. The role of ErbB2 signaling in the onset of terminal differentiation of oligodendrocytes in vivo. J Neurosci 23:5561–5571.
Koprivica V, Cho KS, Park JB, Yiu G, ATwal J, Gore B, Kim JA, Lin E, Tessier-Lavigne M, Ghen DF, He Z. 2005. EGFR activation mediates inhibition of axon regeneration by myelin and chondroitin sulfate proteoglycans. Science 310:106–110.
Knapp PE, Skoff RP. 1987. A defect in the cell cycle of neuroglia in the myelin deficient jimpy mouse. Brain Res 432:301–306.
Kruger L, Bendotti C, Rivolta R, Samanin R. 1992. GAP-43 mRNA localization in the rat hippocampus CA3 field. Mol Brain Res 13:267–272.
Kuhlmann T, Lingfeld G, Bitsch A, Schuchardt J, Bruck W. 2002. Acute axonal damage in multiple sclerosis is most extensive in early disease stages and decreases over time. Brain 125:2202–2212.
Larsen JO, Gundersen HJ, Nielsen J. 1998. Global spatial sampling with isotropic virtual planes: Estimators of length density and total length in thick, arbitrarily orientated sections. J Microsc 191:238–248.
Lee X, Yang Z, Shao Z, Rosenberg SS, Levesque M, Pepinsky RB, Qui M, Miller RH, Chang JR, Mi S. 2007. NGF regulates the expression of axonal LINGO-1 to inhibit oligodendrocyte differentation and myelination. J Neurosci 27:220–225.
Lledo P-M, Alonso M, Grubb MS. 2006. Adult neurogenesis and functional plasticity in neuronal circuits. Nat Rev Neurosci 7:179–193.
Lubetzki C, Demerens C, Anglade P, Villarroya H, Frankfurter A, Lee VM, Zalc B. 1993. Even in culture, oligodendrocytes myelinate solely axons. Proc Natl Acad Sci USA 90:6820–6844.
Ludwin SK, Maitland M. 1984. Long-term remyelination fails to reconsitute normal thickness of central myelin sheaths. J Neurol Sci 64(2):193–198.
Matthews DA, Cotman C, Lynch G. 1976. An electron microscopic study of lesion-induced synaptogenesis in the dentate gyrus of the adult rat. I. Magnitude and time course of degeneration Brain Res 115:1–21.
Mi S, Miller RH, Lee X, Scott ML, Shulag-Morskay SS, Shao Z, Chang J, Thill G, Levesque M, Zhang M, Hession C, Sah D, Trapp B, He Z, Jung V, McCoy JM, Pepinsky RB. 2005. LINGO-1 negatively regulates myelination by oligodendrocytes. Nat Neurosci 8:745–751.
Mihailov GV, Sereda MW, Brinkmann BG, Fischer TM, Haug B, Birchmeier C, Role L, Lai C, Schwab MH, Nave KA. 2004. Axonal neuregulin-1 regulates myelin sheath thickness. Science 304:700–703.
Nielsen HH, Ladeby R, Drøjdahl N, Peterson AC, Finsen B. 2006. Axonal degeneration stimulates the formation of NG2+ cells and oligodendrocytes in the mouse. Glia 54:105–115.
Noppeney U, Friston KJ, Ashburner J, Frackowiak R, Price CJ. 2005. Early visual deprivation induces structural plasticity in gray and white matter. Curr Biol 15:R488–R490.
Raine CS. 1997. In: Raine CS, McFarland HF, Tourtellotte WW, editors. Multiple sclerosis: Clinical and pathogenetic basis. London: Chapman & Hall Medical. p 151–171.
Schwab ME. 2004. Nogo and axon regeneration. Curr Opin Neurobiol 14:118–124.
Sedgwick ME. 1997. Pathophysiology of the demyelinated nerve fibre. In: Raine CS, McFarland HF, Tourtellotte WW, editors. Multiple sclerosis. Clinical and pathogenetic basis, 1st ed. London: Chapman & Hall. pp 197–204.
Seil FJ. 1989. Axonal Sprouting in Response to Injury. Neural regeneration and transplantation. In: Seil FJ, editor. Frontiers of clinical neuroscience, Vol. 6. New York: Alan R. Liss. pp 123–135.
Siddiqui AH, Joseph SA. 2005. CA3 axonal sprouting in kainate-induced chronic epilepsy. Brain Res 1066:129–146.
Smith KJ, Blakemore WF, Murray JA, Patterson RC. 1982. Internodal myelin volume and axon surface area. A relationship determining myelin thickness? J Neurol Sci 55:231–246.
Steward O, Vinsant SL. 1983. The process of reinnervation in the dentate gyrus of the adult rat: A quantitative electron microscopic analysis of terminal proliferation and reactive synaptogenesis. J Comp Neurol 214:370–386.
Suzuki M, Raisman G. 1992. The glial framework of central white matter tracts: Segmented rows of contiguous interfascicular oligodendrocytes and solitary astrocytes give rise to a continuous meshwork of transverse and longitudinal processes in the adult rat fimbria. Glia 6:222–235.
Szuchet S, Polak PE, Yim SH. 1986. Mature oligodendrocytes cultured in the absence of neurons recapitulate the ontogenic development of myelin membranes. Dev Neurosci 8:208–221.
Trapp BD, Nishiyama A, Cheng D, Macklin W. 1997. Differentiation and death of premyelinating oligodendrocytes in developing rodent brain. J Cell Biol 137:459–468.
Trapp BD, Peterson J, Ransohoff RM, Rudick R, Mork S, Bo L. 1998. Axonal transection in the lesions of multiple sclerosis. N Engl J Med 338:278–285.
Wang Z, Colognato H, Ffrench-Constant C. 2007. Contrasting effects of mitogenic growth factors on myelination in neuron-oligodendrocyte co-cultures. Glia 55:537–545.

Watanabe M, Sakurai Y, Ichinose T, Aikawa Y, Kotani M, Itoh K. 2006. Monoclonal antibody Rip specifically recognizes 2′,3′-cyclic nucleotide 3′-phosphodiesterase in oligodendrocytes. J Neurosci Res 84:525–533.

West MJ, Slomianka L, Gundersen HJ. 1991. Unbiased stereological estimation of the total number of neurons in the subdivisions of the rat hippocampus using the optical fractionator. Anat Rec 231:482–497.

Will B, Schmitt P, Dalrymple-Alford J. 1985. Brain plasticity, learning and memory: Historical background and conceptual perspectives. In: Will B, Schmitt P, Dalrymple-Alfrod J, editors. Brain plasticity, learning and memory. Advances in behavioral biology, Vol. 28. New York: Plenum. pp 1–11.

Wirenfeldt M, Dalmau I, Finsen B. 2003. Estimation of absolute microglial cell numbers in mouse fascia dentata using unbiased and efficient cell counting principles. Glia 44:129–139.

Yakovlev PI, Lecours AR. 1966. The myelinogenic cycles of the regional maturation of the brain. In: Minkovski A, editor. Regional development of the brain in early life. Oxford, UK: Blackwell. pp 3–70.

Zimmer J. 1974. Long term synaptic reorganization in rat fascia dentata deafferented at adolescent and adult stages: Observations with the Timm method. Brain Res 76:336–342.